


cambridge.org/mrf

Yucheng Yi¹ , Lu Zhu¹ and Xiaomao Cao²

¹School of Information Engineering, East China Jiao Tong University, Nanchang, Jiangxi, China and ²School of Electronic Information, Wuhan University, Wuhan, Hubei, China

Research Paper

Cite this article: Yi Y, Zhu L, Cao X (2023). Signal fusion research in passive radar based on polarization diversity technology. *International Journal of Microwave and Wireless Technologies* **15**, 410–423. <https://doi.org/10.1017/S175907872200023X>

Received: 17 October 2021
Revised: 27 January 2022
Accepted: 31 January 2022
First published online: 24 February 2022

Key words:

Passive radar; polarization amplitude ratio; polarization diversity; polarization signal fusion based on adaptive weighting

Authors for correspondence:

Yucheng Yi,
E-mail: ycyi@ecjtu.edu.cn;
Lu Zhu,
E-mail: lzhu@ecjtu.edu.cn

Abstract

Polarization diversity technology is an effective method to improve the detection performance of passive radar systems, but the related papers mainly conduct research on the polarization diversity in interference suppression, and there are few studies focusing on the polarization characteristics of the target itself. The work in this paper is divided into two parts. The first part is going to investigate the potential benefits of signal fusion in target polarization-scattering characteristic. The analysis results show that the cross-polarized component of the target scattered echo is not always weaker than the co-polarized component, and the polarization amplitude ratio value is mostly concentrated near 1. This indicates that polarization signal fusion will likely improve target detection performance. The other part introduces a polarization signal fusion method based on the non-coherent integration (P-NCI), but this method is susceptible to the influence of the difference in the signal-to-noise ratio (SNR) of the signal of each polarization channel, resulting in a reduction in the SNR of the fusion signal. The polarization signal fusion method based on adaptive weighting (AW-PSF) can effectively improve the robustness of signal fusion. The experimental results show that AW-PSF has better detection performance compared with single-polarization channel and P-NCI.

Introduction

Passive radar or passive coherent location systems have been a popular topic all over the world. A passive radar system does not have a dedicated transmitter, but it uses broadcast transmitters as illuminators of opportunity to locate and track the targets [1–9]. In the past 20 years, the signals used in the development of passive radar systems have been expanded rapidly. The signals could be analog signals such as frequency-modulated broadcasting [1, 2], or digital signals such as digital video broadcasting [3, 4], digital audio broadcasting [5, 6], WLAN signals [7], LTE signals [8], and China Mobile Multimedia Broadcasting [9–11].

Passive radar systems usually have two types of channels. One is used to receive echo signals of targets called the surveillance channel. The other that receives direct path signals of radio-frequency sources called the reference channel. The surveillance channel contains the low-power reflection echo signals from the targets, high-power direct path signals, and strong reflection echo signals from ground, buildings, and so on. The signal transmitted by an external radio-frequency source usually adopts two polarized modes, namely vertical (V) polarization or horizontal (H) polarization. Conventional passive radar systems use a single-polarized antenna to receive signals. Dual-polarization passive radar (DPPR) systems use two orthogonal-channel polarization antennas to receive signals. In most cases, even in the same transmitting polarization mode, both clutter and target have different receiving polarization states in DPPR systems.

Research studies about polarization diversity in passive radar systems have been reported in recent years. Some studies focused on the frequency modulation signals [12–16], and the others on digital television broadcasting signals [17–20]. These advantages have been demonstrated against different operative geometries as well as exploiting different sources of opportunities. In passive radar systems based on polarization diversity technology, the interference signal strength is much greater than the target signal, and scholars are willing to concentrate more on interference suppression. However, with the continuous improvement in interference suppression algorithms in time domain and spatial domain, in the relatively simple electromagnetic propagation environment, such as the suburban plains, the effect of adding polarization filtering to improve the signal-to-noise ratio (SNR) of the target is no longer obvious. Through experimental research, we found that the polarization amplitude ratio (PAR) of the complex structure target fluctuates drastically [21]. Thus, polarization technology is of great significance for the study of target characteristics. Particularly, exploiting the polarization diversity of the target in non-cooperative illuminations is an interesting topic. Therefore, it is necessary to study the polarization-scattering characteristics of the target and propose the corresponding signal fusion schemes.

The first attempt toward this direction is presented by a simple non-coherent integration (NCI) of range-Doppler (RD) maps obtained at multi-polarized surveillance channels. The polarization NCI (P-NCI) strategy aims at increasing the SNR of the target echo. However, it does not fully consider the influence of the noise signal integration of different polarization channels on the SNR of the fused signal. In this paper, we present a new signal fusion method, specifically devised for DPPR systems. In detail, the polarization-scattering characteristics of the target are analyzed and the detection performance of the radar system under different strategies is compared. These modifications enable an extensive validation to be carried out using both simulated and real data. For the experimental validation, we exploit a dataset collected by DPPR systems based on the China Mobile Multimedia Broadcasting (CMMB) signal, which is equipped with three orthogonal-polarized surveillance antennas and one linearly polarized reference antenna. We demonstrate the benefits of the proposed solution with respect to the conventional passive radar processing performed at the single-polarization channel as well as with respect to P-NCI approaches.

The paper is organized as follows. Section “Signal model” addresses the signal model of DPPR. Section “Electromagnetic simulation” describes the polarization-scattering characteristics of the target, and carries out a statistical analysis on the radar cross-section (RCS) of the target. Section “Polarization signal fusion” proposes the scheme of adaptive weighting-based signal polarization fusion. In Section “Monte Carlo simulation,” the simulation analyses prove that the scheme of adaptive weighting-based signal polarization fusion is effective. Section “Experimental research” shows the experimental results. Section “Conclusion” draws conclusions based on the experimental results and analysis in the previous sections.

Signal model

Passive radar is a special form of bi-static/multi-static radar system. The received signal contains direct path signals, strong clutters, and target echoes. Thus, the measurement of polarization state in echo signals becomes complicated. The composite clutter signal presents partially polarized wave characteristic.

In this paper, the bold letters represent vector and the italic represent scalar. Assume that the received signal noise is Gaussian white noise. Combined with the signal model of passive radar and polarization diversity technology, the echo signals are expressed as Jones vector form:

$$S_j = \begin{bmatrix} E_H \\ E_V \end{bmatrix} = \begin{bmatrix} E_{dh} \\ E_{dv} \end{bmatrix} c_1 d(t) + \sum_{n=2}^{M_c} \begin{bmatrix} E_{nh} \\ E_{nv} \end{bmatrix} c_n d(t - \tau_n) + \sum_{m=1}^{M_t} \begin{bmatrix} E_{mh} \\ E_{mv} \end{bmatrix} \alpha_m d(t - \tau_m) e^{j2\pi f_m^D t} + \begin{bmatrix} w_h \\ w_v \end{bmatrix} \tag{1}$$

where $d(t)$ is the transmitted signal. E_{dh} , E_{nh} , and E_{mh} represent the H polarization component of the direct path signal, clutters, and targets, respectively. E_{dv} , E_{nv} , and E_{mv} represent the V polarization component of the direct path signal, clutters, and targets, respectively. w_h and w_v represent the Gaussian white noise of the H channel and V channel, respectively. c_1 , c_n and α_m represent the amplitude of the direct path signal, clutters, and targets, respectively. τ_n and τ_m represent the delay with respect to the direct path signal. f_m^D represents the Doppler frequency of the m -th target. M_c and M_t represent the number of clutters and targets, respectively.

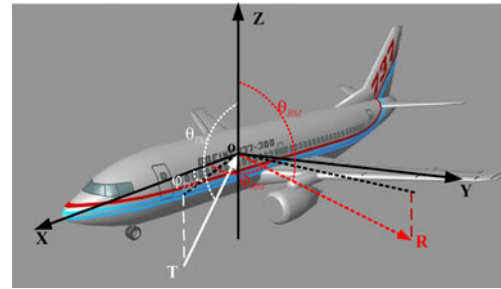


Fig. 1. Electromagnetic calculation coordinate.

E_H and E_V can be represented in (2) and (3), respectively:

$$E_H = a_h(t) e^{j\phi_h} \tag{2}$$

$$E_V = a_v(t) e^{j\phi_v} \tag{3}$$

where $a_h(t)$ and $a_v(t)$ represent the amplitude of signal model in the H channel and V channel. ϕ_h and ϕ_v represent the phase of signal model in the H channel and V channel.

Electromagnetic simulation

RCS of Boeing 737

Boeing 737 is the main aircraft type of China Airlines, and it is also one of the aircraft types that can often be observed in detection experiments of passive radar. Therefore, in order to study the target bi-static polarization-scattering characteristics of the digital television broadcasting band, this section will use this aircraft type to establish an electromagnetic calculation model. The target electromagnetic calculation coordinate is shown in Fig. 1.

In Fig. 1, the angle between the clockwise direction of the incident electromagnetic wave and the z-axis is defined as the incident pitch angle θ_{TM} , and the value is 0–180°. The angle between the projection of the incident electromagnetic wave in the XOY plane in the clockwise direction and the x-axis is defined as the incident azimuth angle φ_{TM} , and the value is 0–360°. Similarly, we define the pitch angle and azimuth angle of the scattered electromagnetic wave. Taking CMMB signal as an example, the center frequency is set as 714 MHz. The calculation software used is High Frequency Structure Simulator (HFSS). The simulation results can guide the experimental research of DPPR system target detection based on the cyclic prefix-orthogonal frequency division multiplexing (CP-OFDM) signal.

Assuming that the target is located in the far-field area, and the polarization components of the incident electromagnetic wave and the scattered electromagnetic wave satisfy a linear relationship, then the polarization-scattering matrix can be used to describe the polarization characteristics of the target [22]. The Jones vector is used to describe the incident electromagnetic wave as, $E_T = [E_{TH} \ E_{TV}]^T$, the scattering electromagnetic wave as, $E_R = [E_{RH} \ E_{RV}]^T$. The polarization-scattering matrix of target can be defined as:

$$S = \begin{bmatrix} S_{HH} & S_{VH} \\ S_{HV} & S_{VV} \end{bmatrix} \tag{4}$$

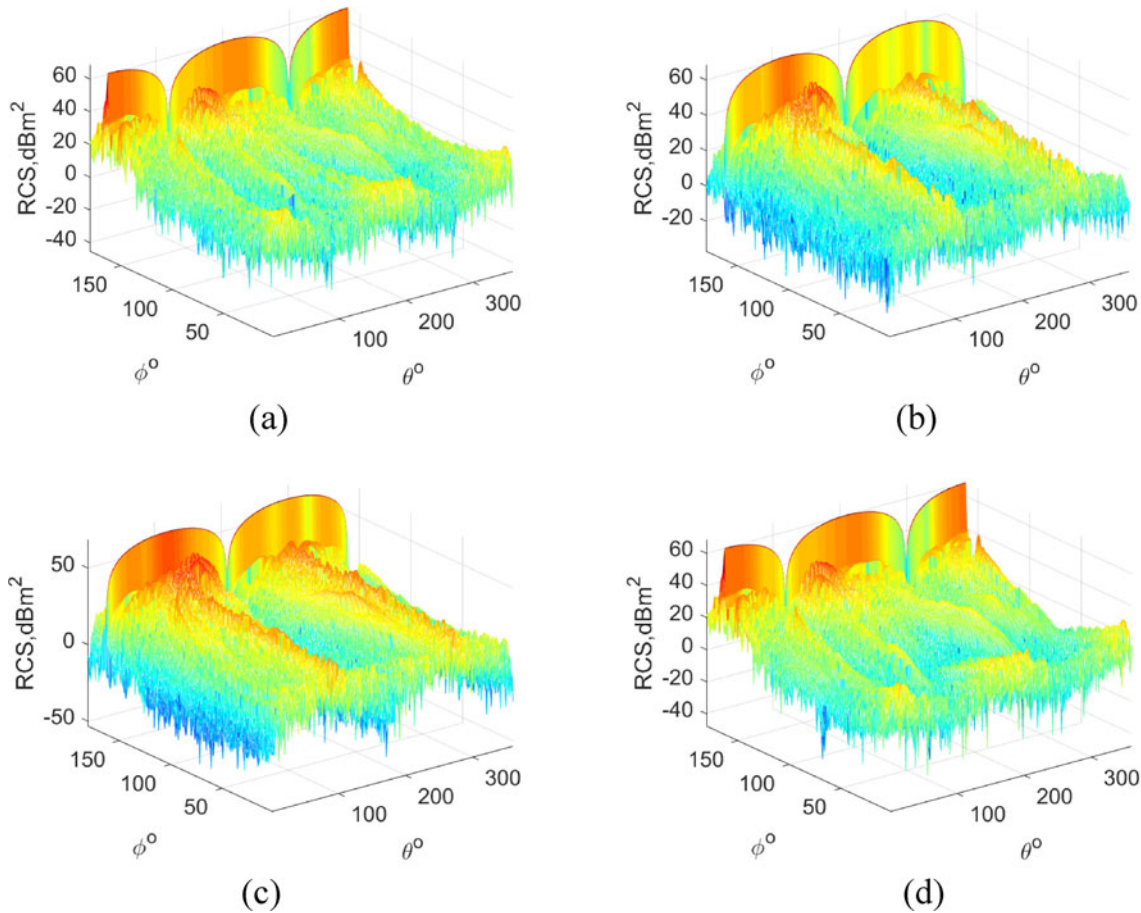


Fig. 2. Electromagnetic simulation results of HFSS incident on the abdomen of Boeing 737: (a) HH polarization, (b) VH polarization, (c) HV polarization, and (d) VV polarization.

and

$$E_R = S \cdot E_T \tag{5}$$

where S_{VH} represents the V component of the scattered electromagnetic wave when the H-polarized electromagnetic wave illuminates the target. Under the conditions of known incident electromagnetic wave frequency and target attitude, the bi-static RCS can be expressed as:

$$\sigma_{ij}(f, \theta_{TM}, \varphi_{TM}, \theta_{RM}, \varphi_{RM}) = 4\pi |S_{ij}(f, \theta_{TM}, \varphi_{TM}, \theta_{RM}, \varphi_{RM})|^2 \tag{6}$$

where $i, j = H, V$, f represents incident electromagnetic wave frequency.

Assuming that the electromagnetic waves are incident from the abdomen, nose, and left side of Boeing 737, the scattering RCS are shown in Figs 2–4. The specific parameters are shown in Table 1.

It can be observed from Figs 2–4, irrespective of the direction the incident electromagnetic wave illuminates the aircraft, the target bi-static RCS of different polarizations changes dramatically with the pitch angle and azimuth angle of the scattered electromagnetic wave. The RCS of the four polarization receiving and transmitting modes presents a symmetrical distribution. When the target is located in the forward scattering area, the RCS of orthogonal polarization scattering is much smaller than the

RCS of co-polarization scattering. In Fig. 3, by comparing the two modes of VH polarization and HV polarization, we find that the VH polarization mode will form a depression near $\theta = 90^\circ$, which indicates that Boeing 737 has better cross-polarization-scattering RCS for the V polarized incident wave.

Statistical analysis

Common statistical parameters, such as mean, standard deviation, maximum, minimum, range, etc., can be used to describe the fluctuation characteristics of target RCS more intuitively. When the frequency of the incident electromagnetic wave is constant, the characteristics of various parameters of the target within different bi-static angle ranges are calculated, and the length of each segment of statistical data is M , then the mean can be defined as the average value of the data D :

$$\bar{\delta} = \frac{1}{M} \sum_{m=1}^M \delta_n \tag{7}$$

The standard deviation of the data D can be expressed as:

$$\sigma = \sqrt{\frac{\sum_{m=1}^M (\delta_n - \bar{\delta})^2}{M - 1}} \tag{8}$$

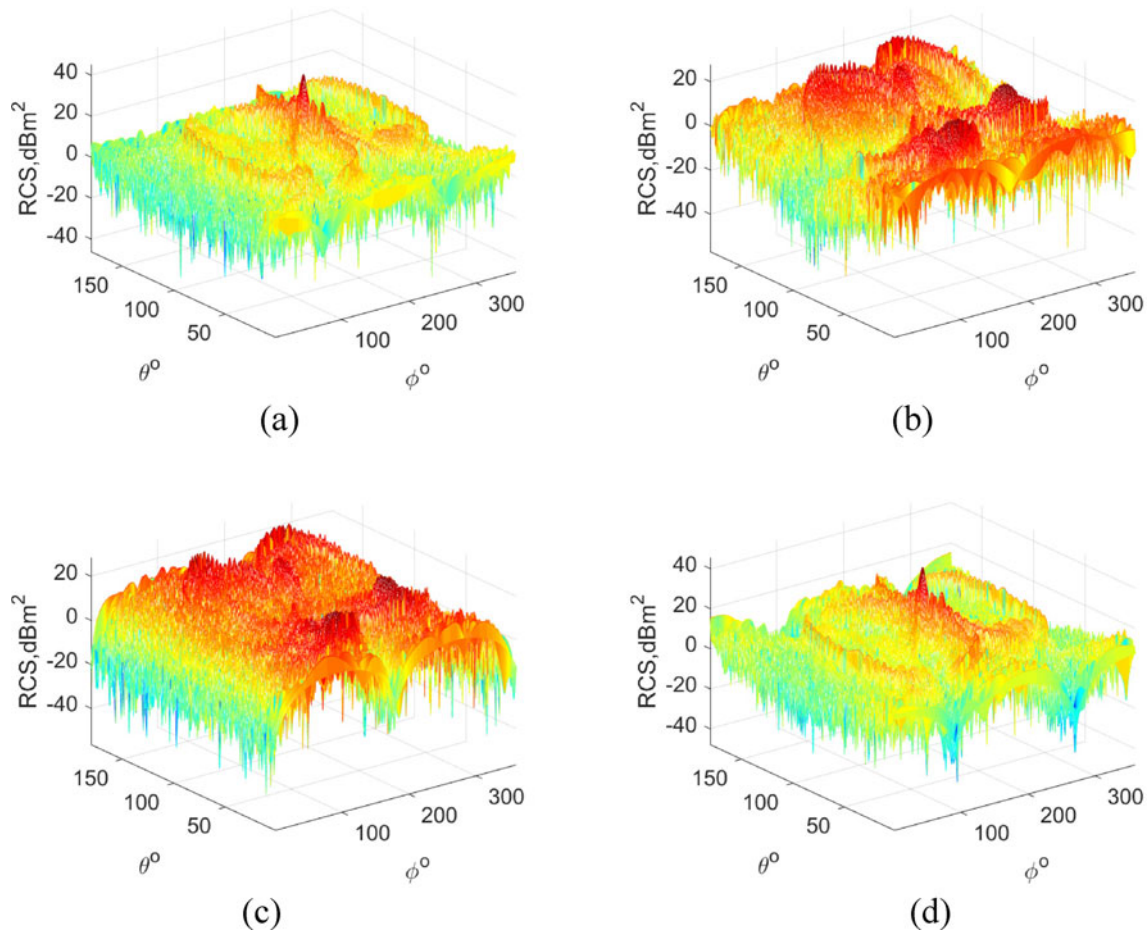


Fig. 3. Electromagnetic simulation results of HFSS incident on the nose of Boeing 737: (a) HH polarization, (b) VH polarization, (c) HV polarization, and (d) WV polarization.

The maximum value of the data D can be expressed as:

$$\delta_{\max} = \max \{\delta_m\}, \quad m = 1, 2, \dots, M \tag{9}$$

The minimum value of the data D is:

$$\delta_{\min} = \min \{\delta_m\}, \quad m = 1, 2, \dots, M \tag{10}$$

The range is defined as the difference between the maximum and minimum:

$$\delta_c = \delta_{\max} - \delta_{\min} \tag{11}$$

Taking the incident electromagnetic wave in the abdomen model as an example, after the simulation data are normalized, the bi-static RCS approximate probability density (PD) histogram can be obtained through statistical analysis (Fig. 5).

According to the coordinate system shown in Fig. 1, the bi-static angle of passive radar can be expressed as:

$$\begin{aligned} \cos \beta &= \sin \theta_{TM} \cos \varphi_{TM} \sin \theta_{RM} \cos \varphi_{RM} \\ &+ \sin \theta_{TM} \sin \varphi_{TM} \sin \theta_{RM} \sin \varphi_{RM} + \cos \theta_{TM} \cos \theta_{RM} \end{aligned} \tag{12}$$

When the electromagnetic wave incident angle is $(\varphi_{TM}, \theta_{TM})$, the relationship between the bi-static angle and the electromagnetic

wave scattering angle $(\varphi_{RM}, \theta_{RM})$ can be obtained from (12). Also, when $\theta_{TM} = 180^\circ$, and the statistical results of the mean, standard deviation, maximum and minimum of the target bi-static RCS are shown in Fig. 6.

In Fig. 6(a), the trend of the bi-static RCS mean is basically the same. When the bi-static angle is 0° , the mean of the target RCS is not the maximum. When the bi-static angle is 180° , the mean of the target RCS is the largest. When the bi-static angle is between 50° and 150° , the mean of the RCS in different polarization modes satisfies $RCS_{m_VH} > RCS_{m_HV} > RCS_{m_HH} > RCS_{m_VV}$. In Fig. 6(b), the trend of fluctuation in the bi-static RCS standard deviation is lower than the mean, and the variation trend of the RCS standard deviation in HH polarization and VV polarization are similar, the same as VH polarization and HV polarization. But, the RCS standard deviation in VH polarization and HV polarization are significantly largest than the ones in HH polarization and VV polarization which show that the RCS fluctuates obviously in the VH polarization and HV polarization, and it indicates that in the two polarization modes the target SNR fluctuates sharply. In Fig. 6(c), when the bi-static angle $\beta = 180^\circ$, the maximum is the largest. The difference in the maximum of RCS between the two co-polarization modes and the two cross-polarization modes is obvious. As show in Fig. 6(d), the RCS minimum fluctuates greatly with each change of the bi-static angle. The overall observation shows that, except for the smaller RCS minimum in the HV polarization mode, the difference in the RCS of the

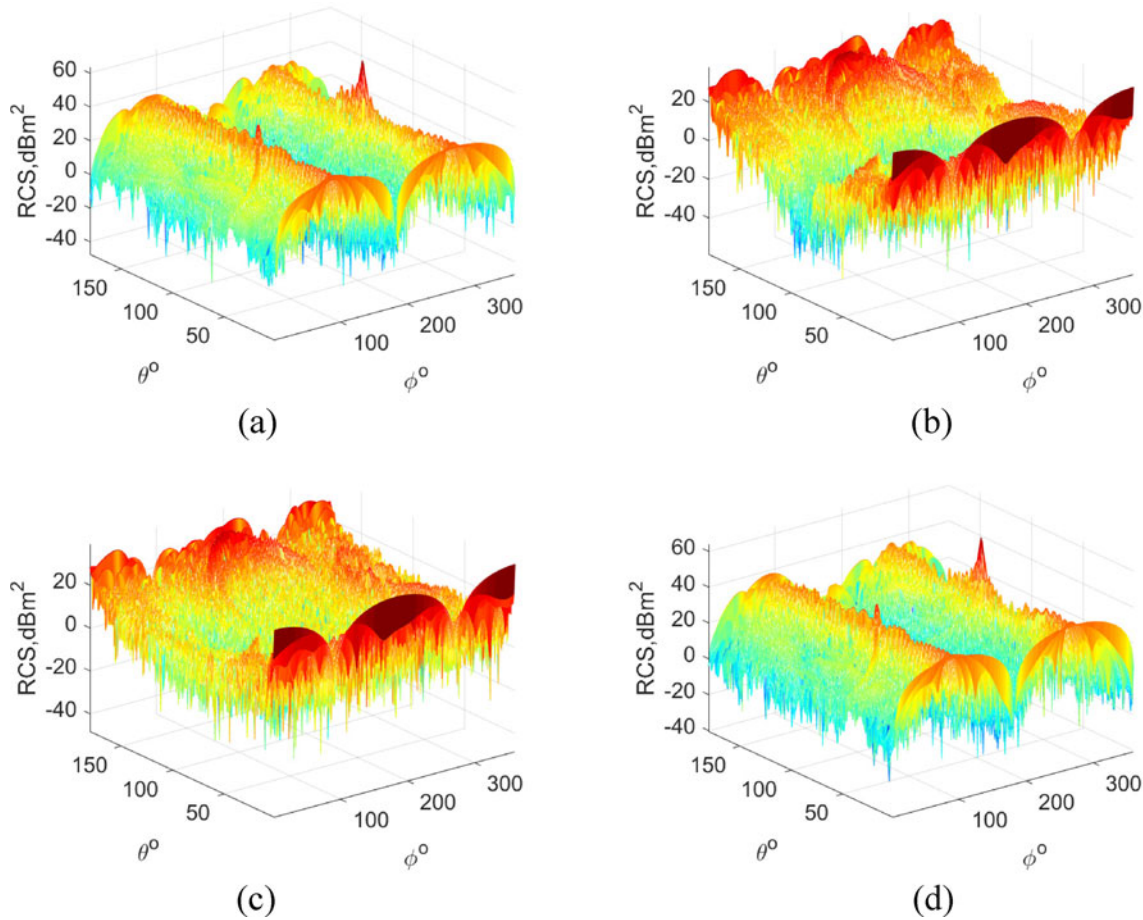


Fig. 4. Electromagnetic simulation results of HFSS incident on the left side of Boeing 737: (a) HH polarization, (b) VH polarization, (c) HV polarization and (d) VV polarization.

Table 1. Incident and scattering direction description

	Figure 2	Figure 3	Figure 4
Incident direction	$\varphi_{TM} = 0^\circ,$ $\theta_{TM} = 180^\circ$	$\varphi_{TM} = 0^\circ,$ $\theta_{TM} = 90^\circ$	$\varphi_{TM} = 90^\circ,$ $\theta_{TM} = 90^\circ$
Scattering direction	$\varphi_{RM} = 0-360^\circ$ $\theta_{RM} = 0-180^\circ$	$\varphi_{RM} = 0-360^\circ$ $\theta_{RM} = 0-180^\circ$	$\varphi_{RM} = 0-360^\circ$ $\theta_{RM} = 0-180^\circ$

other three polarization transmission and reception modes is not obvious. The statistical analysis presented in Figs 6(c) and 6(d) shows that the RCS fluctuation of the orthogonal polarization mode is more severe, which is the same as the analysis conclusion from Fig. 6(b).

Polarization amplitude ratio

Polarization ratio is a very important electromagnetic wave polarization descriptor [23], assuming that the incident electromagnetic wave is vertically polarized, it is defined as follows:

$$\rho_{HV} = \frac{E_H}{E_V} = |\rho_{HV}|e^{j\phi_{HV}} \tag{13}$$

where E_V and E_H represent the electric field components of the horizontal channel and the vertical channel of the receiving

antenna, respectively; and ϕ_{HV} represents the phase difference between the horizontal and vertical channel.

In the US Patent “Polarized radar system for providing target identification and discrimination” [24] (number 4035797), the author proposes that for simple targets, the ratio of the co-polarization and cross-polarization signal amplitudes is a constant, while for complex targets, the ratio changes with different detection distances. The formula to calculate the PAR is:

$$PAR_{HV} = |\rho_{HV}| \tag{14}$$

A statistical analysis was performed on the characteristics of the target PAR using HFSS, and the resulting histogram is shown in Fig. 7.

It can be observed from the four statistical histograms that the PD values of the PAR are concentrated around 1. Calculate the proportion of $PAR_{VH/HH}$, $PAR_{HV/VV}$, $PAR_{HV/VH}$ and $PAR_{VV/HH}$ values less than or equal to 1 respectively, and the results are shown in Table 2.

The $PAR_{VH/HH}$ represents the amplitude ratio of the V component and the H component of the scattered electromagnetic wave when the incident electromagnetic wave is H polarized. The $PAR_{HV/VV}$ represents the amplitude ratio of the H component and the V component of the scattered electromagnetic wave when the incident electromagnetic wave is V polarized. $PAR_{HV/VH}$ and $PAR_{VV/HH}$ are defined similarly. In Table 2, when the

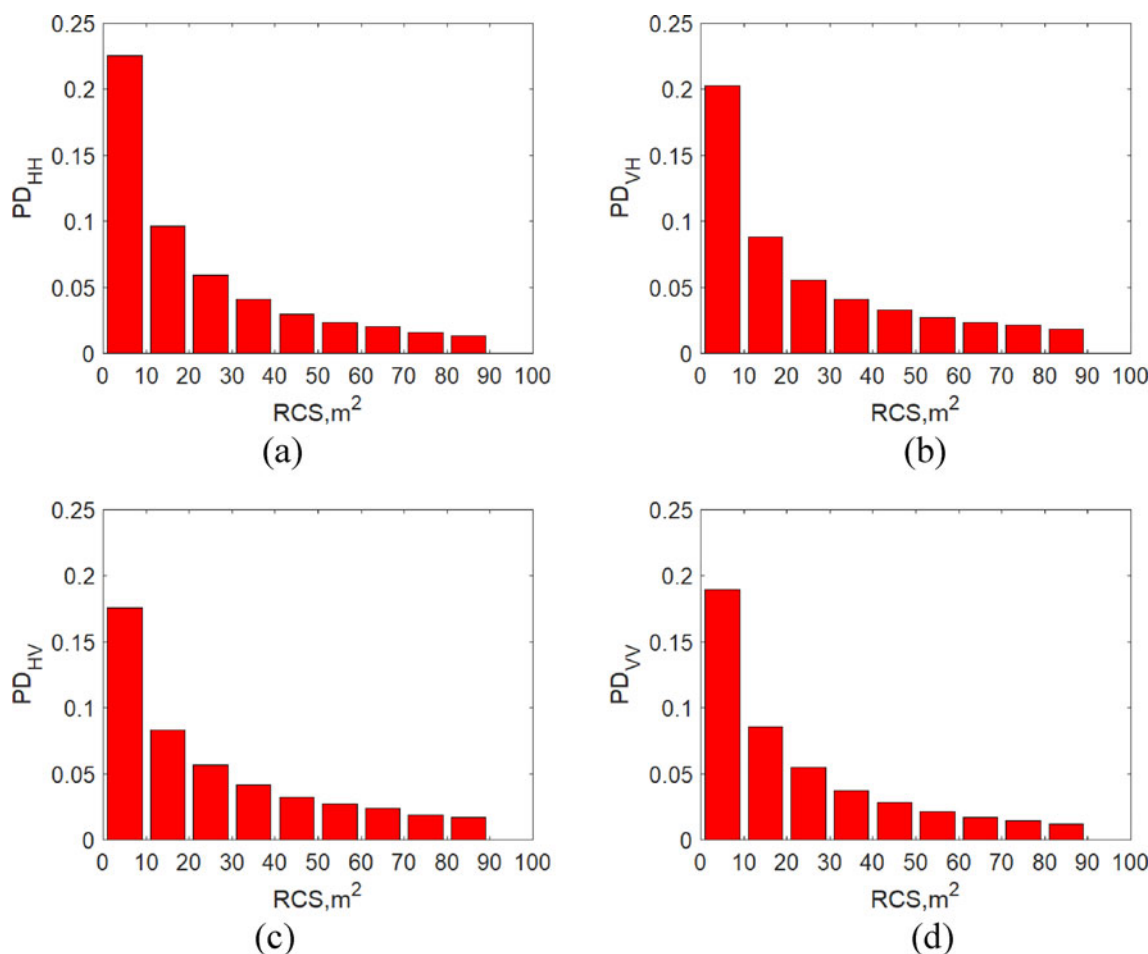


Fig. 5. Bistatic RCS PD statistics results: (a) HH polarization, (b) VH polarization, (c) HV polarization and (d) VV polarization.

polarization mode of the incident electromagnetic wave is fixed (H or V), the PD value of the cross-polarization component is weaker than the co-polarization component in the scattered echo and is close to 0.5. It is shown that the cross-polarization component is as important as the co-polarization component. It is possible to improve the detection performance of a radar system by using polarization diversity technology.

Target dynamic analysis

In the earlier research, the analysis of the polarization-scattering characteristics of the target was based on the reasonable design of the pitch angle θ_{TM} , the azimuth angle φ_{TM} of the incident electromagnetic wave, and the pitch angle θ_{RM} and the azimuth angle φ_{RM} of the scattered electromagnetic wave. This cannot fully reflect the changes in the scattering characteristics of the target during a flight. In order to obtain more realistic simulation result, we use decoding and interpolation methods to extract the longitude, latitude, altitude, and other information of the target at all times from the automatic dependent surveillance-broadcast (ADS-B) signal of the actual route, and the location and altitude information of the transmitter and DPPR system are known. Therefore, we can calculate the electromagnetic wave incident angle from the transmitter to the target and the electromagnetic wave scattering angle from the target to the radar antennas. Regardless of various attenuation factors, using electromagnetic simulation data, the fluctuation state of

the target RCS and PAR can be obtained closer to the real scene. The screenshot of the target in the ADS-B system is shown in Fig. 8. The relative positions of the transmitter, receiver, and target are indicated in Fig. 8.

As shown in Fig. 9, when the incident electromagnetic wave is in H polarization, the cross-polarization component of the target RCS is smaller than the one of co-polarization components; when the incident electromagnetic wave is in V polarization, the RCS of target in the cross-polarization component is larger than the one of co-polarization components at certain moments.

Figure 10 shows the PAR of the target in different polarization modes of the incident electromagnetic wave. When the incident electromagnetic wave is in V polarization, the target PAR fluctuates around 0 dB.

The ADS-B system provides information on the position of the target at 23 different times. The relationship between the cross-polarization and co-polarization components in RCS and PAR of scattered echo is shown in Table 3. In Table 3, number represents the number of times when the cross-polarization component of RCS is greater than or equal to the co-polarization component in the 23 times. The proportion indicates the proportion of the PAR greater than or equal to 0 dB when the incident electromagnetic wave is in H or V polarization. When the incident electromagnetic wave is in V polarization, both RCS and PAR indicate that the cross-polarization component is slightly stronger than the co-polarization component of scattered echo.

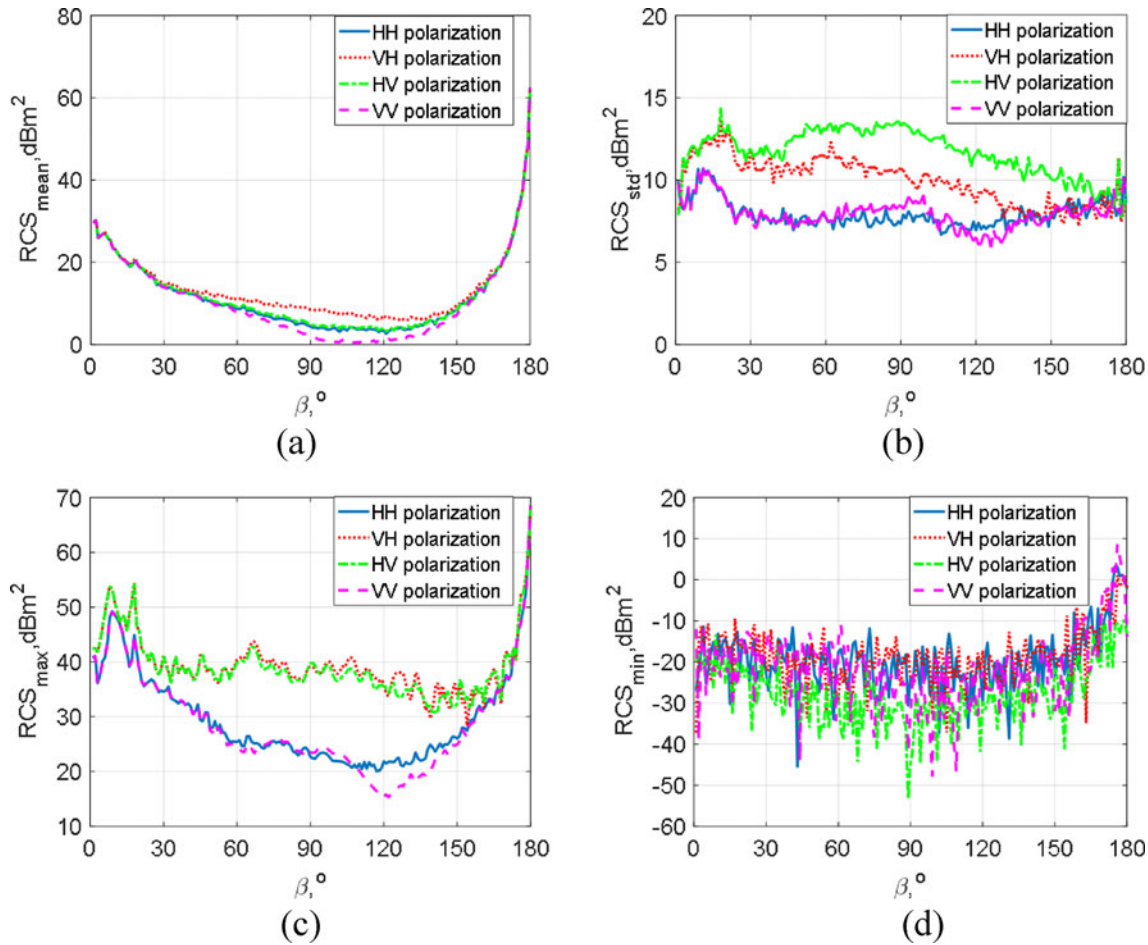


Fig. 6. Bistatic RCS statistical results: (a) mean of bistatic RCS, (b) standard deviation of bi-static RCS, (c) maximum of bistatic RCS, and (d) minimum of bistatic RCS.

In China, most broadcast and television signals are transmitted in V polarization. Therefore, the use of target polarization fusion will likely improve the performance of the DPPR system.

Polarization signal fusion

Polarization non-coherent integration

In the research of passive radar based on polarization diversity technology, most of the research results are concentrated in the use of polarization diversity to suppress interference and clutter [9, 14, 21]. However, the flicker of the target RCS will seriously affect the detection performance of the conventional single-polarization passive radar. Using the polarization fusion technology, the purpose of improving the performance of the signal of the passive radar can be achieved [17]. The advantage of DPPR over conventional single-polarization passive radar depends on the improvement of the SNR brought by target signal polarization fusion. We can set-up a simple simulation scenario: assume that there is a group of target polarization-scattering echo data; the SNR of each echo signal before coherent accumulation is -45 dB, the coherent accumulation time is 0.1 s; the bandwidth of the signal is 8 MHz, and the polarization angle of each echo signal follows the uniform distribution $U(0^\circ, 90^\circ)$. The cell-average constant false-alarm rate (CA-CFAR) method is adopted, and the false-alarm rate is 10^{-6} .

Assume that the RD maps of K polarization surveillance channels are denoted as $RD_k(\tau, \nu)$ ($k=1, \dots, K$). If the cell under test is located in the distance cell τ_0 and the Doppler cell ν_0 , the cell under test in the K channels form a complex vector $\mathbf{x}_0 = [RD_1(\tau_0, \nu_0) \dots RD_K(\tau_0, \nu_0)]^T$. The noise of each polarization channel satisfies the condition of independent and identical distribution, and \mathbf{x}_0 satisfies a normal distribution with zero mean under the assumption of H_0 . In the assumption of H_1 (target and noise), $\mathbf{x}_t = [RD_1(\tau_t, \nu_t) \dots RD_K(\tau_t, \nu_t)]^T$, where τ_t and ν_t represent the distance cell and the Doppler cell of target, respectively. The authors in [17] and [25] studied the effect of P-NCI fusion method on the performance of a PDPR system based on digital video broadcasting-terrestrial (DVB-T) and frequency modulated (FM) signals. When the cell under test of RD map in the k polarization channels is processed by square-law detection and NCI, the result is:

$$y_{P-NCI}(\tau_0, \nu_0) = |\mathbf{x}_0|^2 = \sum_{k=1}^K |RD_k(\tau_0, \nu_0)|^2 \quad (15)$$

and the q -th reference cell can be represented as

$$y_{P-NCI}(\tau_q, \nu_q) = \sum_{k=1}^K |RD_k(\tau_q, \nu_q)|^2 \quad (16)$$

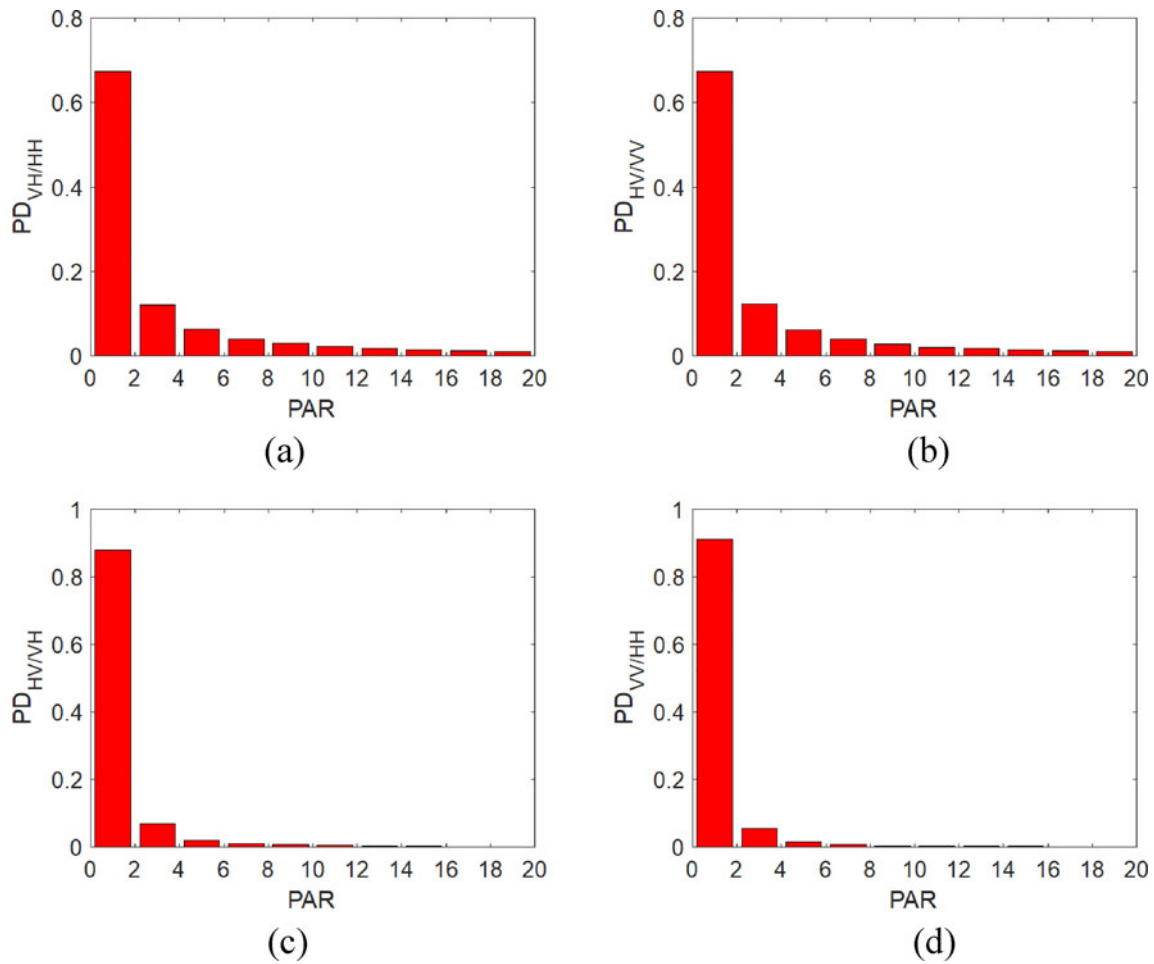


Fig. 7. PAR statistics histogram: (a) VH/HH, (b) HV/VV, (c) HV/VH and (d) VV/HH.

Table 2. Statistical result

	$PAR_{VH/HH} \leq 1$	$PAR_{HV/VV} \leq 1$	$PAR_{HV/VH} \leq 1$	$PAR_{VV/HH} \leq 1$
PD value	0.453	0.454	0.596	0.591

The decision criterion of the CA-CFAR detector based on the P-NCI fusion method is:

$$\frac{y_{P-NCI}(\tau_0, v_0)}{\sum_{q=1}^Q y_{P-NCI}(\tau_q, v_q)} \begin{matrix} > T \\ < T \end{matrix} \begin{matrix} H_1 \\ H_0 \end{matrix} \quad (17)$$

The threshold factor T can be obtained by setting the theoretical false-alarm probability as in (18) [26]:

$$P_{fa} = \sum_{k=0}^{K-1} \binom{MK+k-1}{k} \left(\frac{T}{MT}\right)^k \left(1 + \frac{T}{MK}\right)^{-MK-k} \quad (18)$$

where M is the number of secondary cells and T is the CFAR threshold.

As shown in Fig. 11, the detection effect of CA-CFAR detector based on P-NCI is improved compared to the every single-

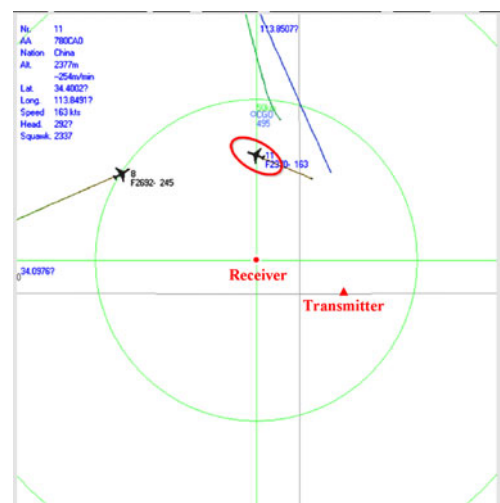


Fig. 8. Screenshot of ADS-B system.

polarization channel. But, there are still some trace points that cannot be detected. This is caused by the difference in the SNR of the echo signal between different polarization channels. However, the received signal of the V polarization channel is represented as $S_V = s_v + n_v$ and the signal of the H polarization

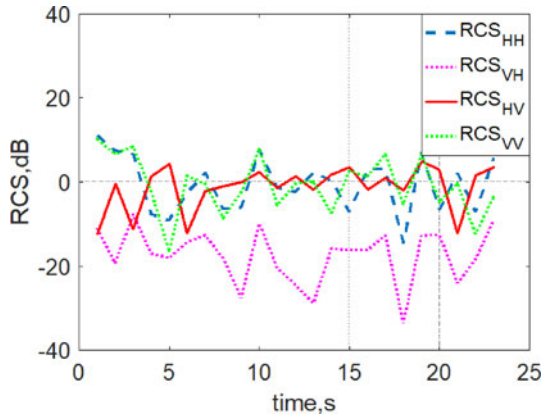


Fig. 9. RCS simulation results in real scenarios.

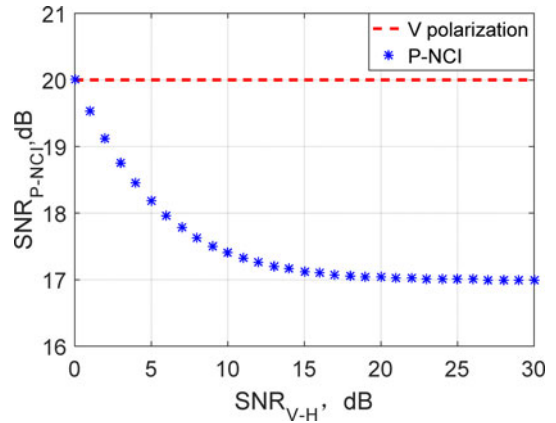


Fig. 12. Influence of SNR difference of each polarization channel on signal fusion based on P-NCI.

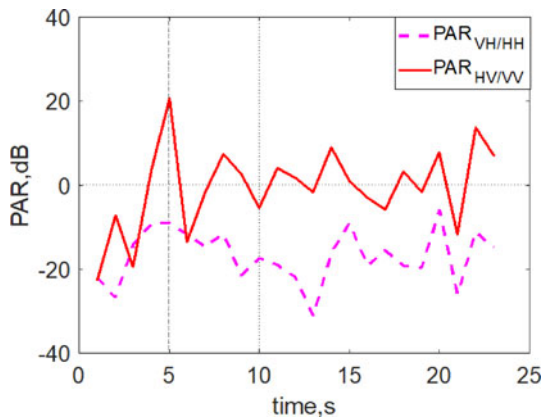


Fig. 10. PAR simulation results in real scenarios.

Table 3. Statistical analysis

	$RCS_{VH} \geq RCS_{HH}$	$RCS_{HV} \geq RCS_{VV}$	$PAR_{VH/HH} \geq 0$ dB	$PAR_{HV/VV} \geq 0$ dB
Number	0	12	-	-
Proportion (%)	-	-	0	52.2

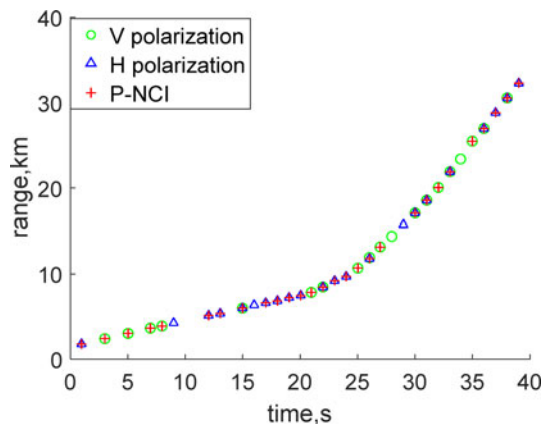


Fig. 11. Detection result of CA-CFAR based on P-NCI.

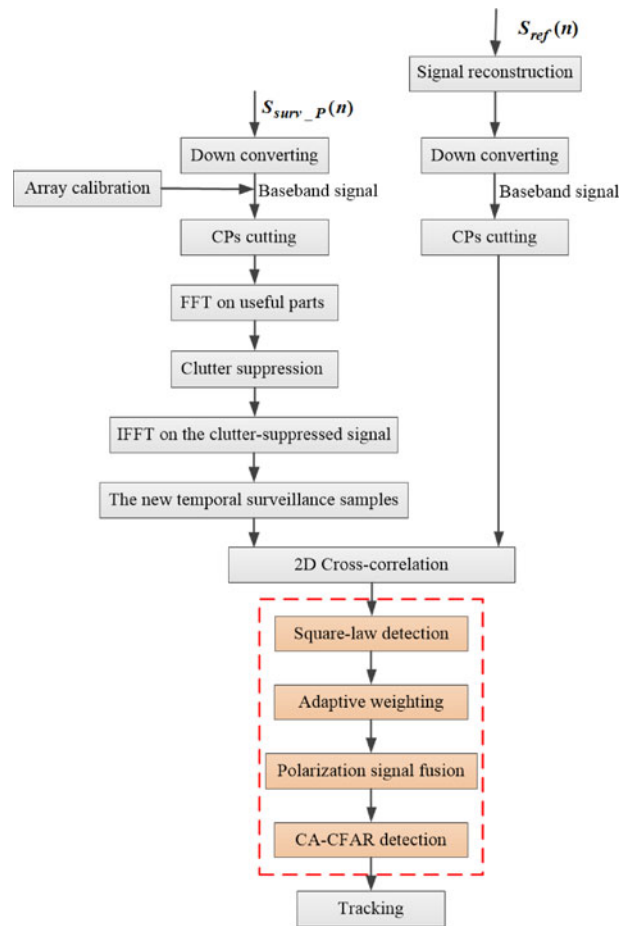


Fig. 13. Signal processing flow of subcarrier-based polarization filtering method.

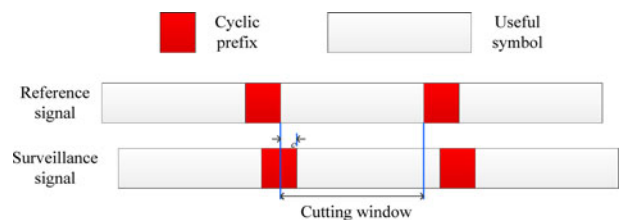


Fig. 14. CPs cutting.

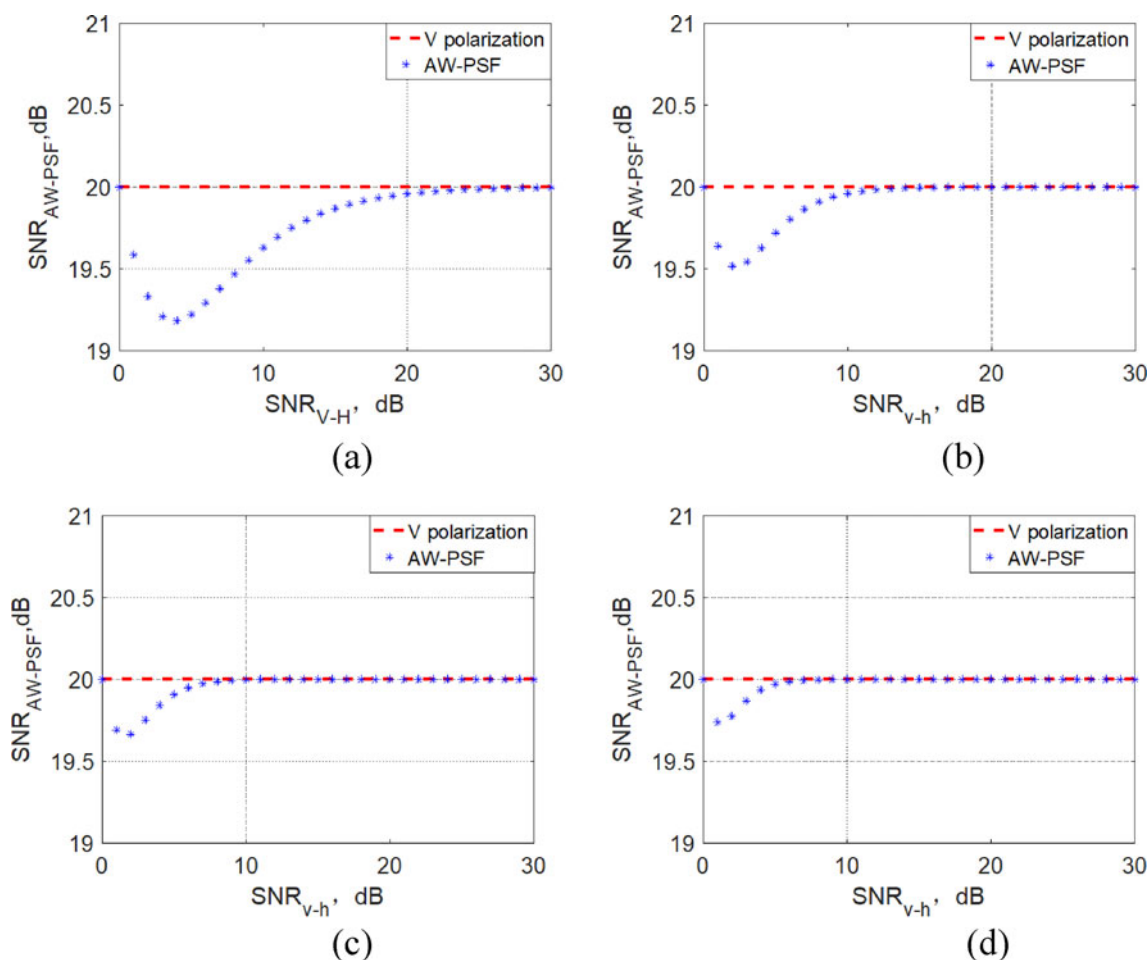


Fig. 15. Influence of different values of n on the AW-PSF method: (a) $n = 1$, (b) $n = 2$, (c) $n = 3$, and (d) $n = 4$.

channel as $S_H = s_h + n_h$. Assuming that $SNR_V = s_v/n_v > SNR_H = s_h/n_h$, then the SNR of fusion signal satisfies $SNR_V > SNR_f > SNR_H$. This may cause the detection result of the fusion signal to be inferior to that of the V polarization channel.

Taking the H and V polarization channels as example, assuming that the average noise floor of the two channels is equal, when the SNR of H channel decreases gradually, $SNR_H \leq SNR_V = 20$ dB, that is, the difference between the H polarization channel and V polarization channel increases gradually; the change in the SNR after subjected to P-NCI is shown in Fig. 12.

Figure 12 shows that the difference in SNR between V and H polarized channel will result in a decrease in SNR of P-NCI.

Signal fusion in polarization weighted

This section will attempt to address the problem raised above by using polarization signal fusion based on adaptive weighted (AW-PSF). Taking a digital television signal based on CP-OFDM as an example, the CP is usually assumed to be greater than or equal to the channel delay extension so as to avoid inter-symbol interferences and assure inter-carrier orthogonal. When this assumption is satisfied, the benefits related to CP for communication purpose could also be derived as advantages for passive radar application. The processing flow is shown in Fig. 13.

It is necessary to pre-process the signal of each polarization channel before signal fusion. The signal of opportunistic illumination source is received by the reference antenna, and we need to perform signal reconstruction to obtain a pure reference signal [27]. In order to ensure the consistency of the amplitude and phase between the surveillance antennas of polarization array, it is necessary to calibrate the antennas first. Then, it is necessary to perform CPs cutting on the echo signal of each channel. The CP cutting is shown in Fig. 14. τ_c represents the clutter delay. There are two identical synchronous signals at the beginning of each time slot. The content of synchronous signal transmission is known in advance. The starting point of each time slot of the receiving signal can be determined by synchronous signals. According to the CP-OFDM signal structure, the window function can effectively intercept useful symbols. Next, we need to filter the signals in each polarization surveillance channel to remove the interference and clutter signals. Finally, we need to use the reference signal and the surveillance signal to perform matched-filtering processing to obtain the RD maps.

After obtaining RD maps of each polarization channel signal, we need to carry out signal fusion processing. After interference suppression and matched filtering, the data on the RD map of the k -th polarization channel is assumed to be $RD_k(\tau, \nu)$. After the square-law detection processing, the k -th channel and the

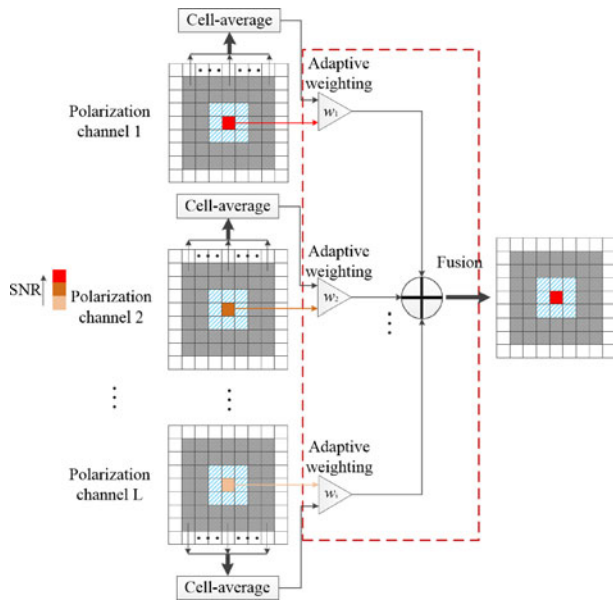


Fig. 16. AW-PSF realization principle diagram.

Table 4. Simulation condition

Carrier frequency	SNR of target	Antenna	False-alarm rate	Monte Carlo
714 (MHz)	15:30 (dB)	3	10^{-6}	500

m -th cell to be detected is $RD_k(\tau_m, \nu_m)$, and the output signal of AW-PSF is defined as:

$$y_{AW-PSF}(\tau_m, \nu_m) = \sum_{k=1}^K (w_{k,m})^n |RD_k(\tau_m, \nu_m)|^2 \quad (19)$$

where

$$w_{l,m} = \frac{|RD_L(\tau_m, \nu_m)|^2 - \overline{|n_{l,m}|^2}}{\overline{|n_{l,m}|^2}} \quad (20)$$

where $\overline{|n_{l,m}|^2}$ represents the average value of the reference cell samples of the l -th channel and the m -th cell to be detected after the square-law detection.

With the same simulation condition as in Fig. 11, and in view of the different values of n in w , the influence of the difference in the SNR of the signal of each polarization channel on the AW-PSF method is evaluated, as shown in Fig. 15.

It can be observed from Fig. 15 that regardless of the value of n , the difference in the SNR between H polarization and V polarization channels has less impact on AW-PSF compared to P-NCI. In different polarization channels, the greater the SNR_{AW-PSF} difference, the better the SNR_{AW-PSF} convergence ($SNR_V > SNR_H$), and the more stable it is. The value of n affects the convergence rate of SNR_{AW-PSF} . The larger the value of n is, the faster the convergence rate is. The AW-PSF method when $n = 1$ is compared with P-NCI in subsequent simulation and experimental analysis. The principle of AW-PSF is shown in Fig. 16.

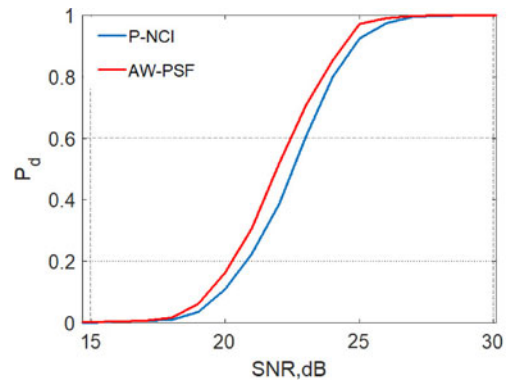


Fig. 17. Relationship between SNR and detection probability.

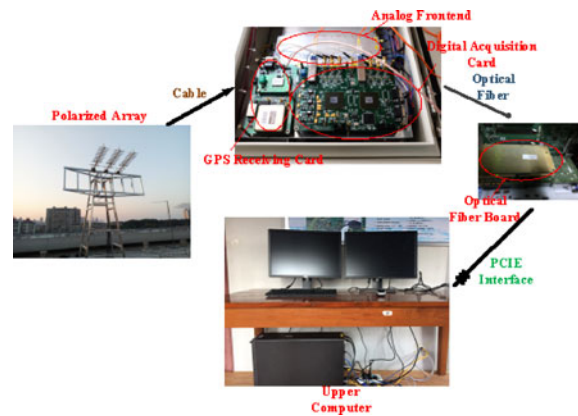


Fig. 18. Polarization diversity passive radar system.

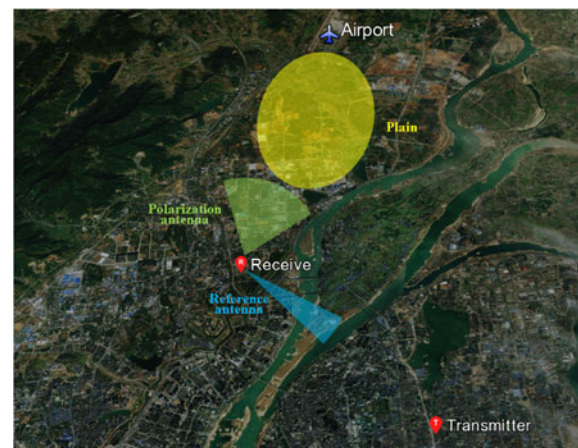


Fig. 19. Experimental geometry and scenario in Nanchang.

Monte Carlo simulation

In order to compare the detection performance of AW-PSF and P-NCI methods, we will conduct Monte Carlo simulation experiment. The simulation conditions are shown in Table 4.

The false-alarm rate is 10^{-6} , and the threshold factor T can be obtained from (18). After performing 500 Monte Carlo simulation experiments, the relationship between the SNR and detection probability is shown in Fig. 17.

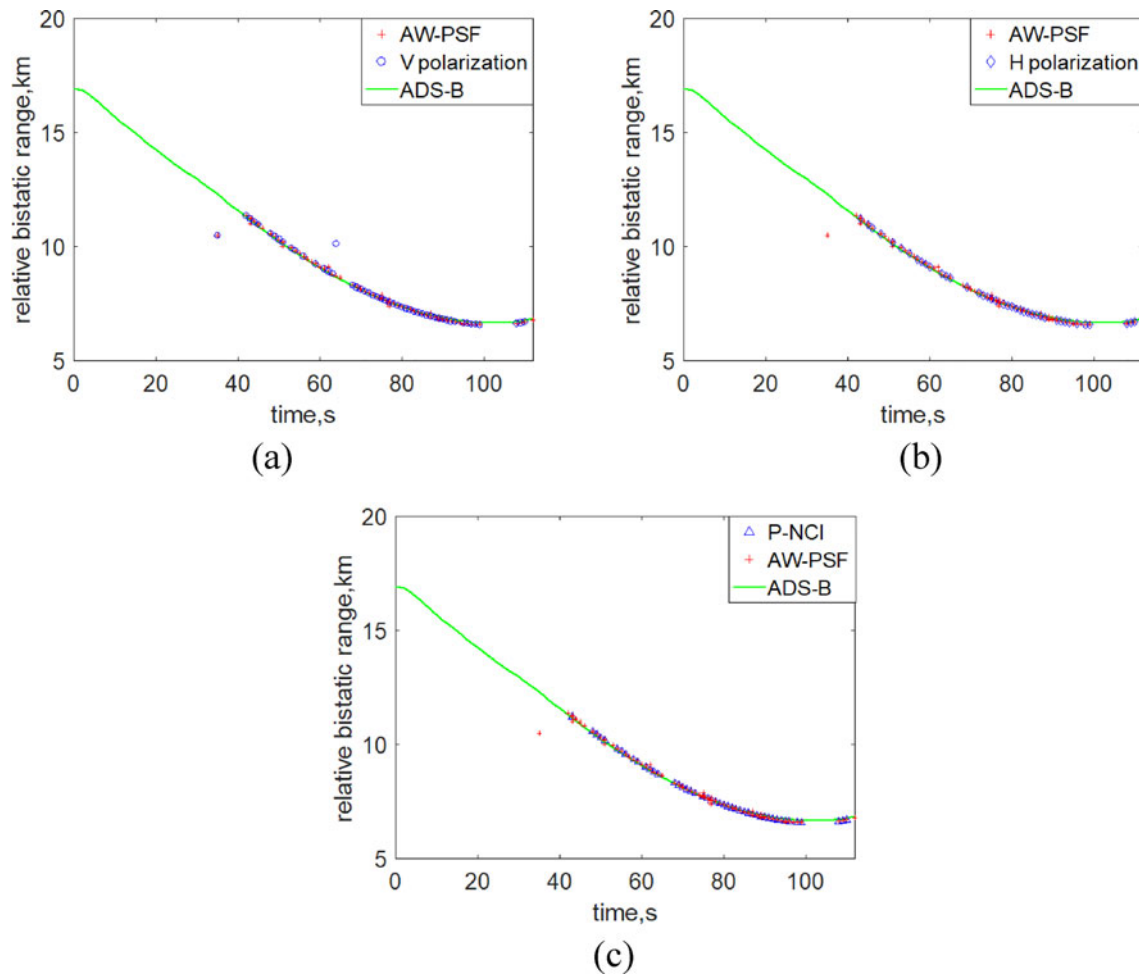


Fig. 20. Comparison of detection results: (a) V polarization and AW-PSF, (b) H polarization and AW-PSF, and (c) P-NCI and AW-PSF.

In Fig. 17, the abscissa is the SNR of signal after matched filtering, and the ordinate is the detection probability of the signal. The AW-PSF method overcomes the adverse effect of SNR difference in different polarization channels on signal fusion, and has better robustness.

Experimental research

Experimental system

DPPR is a special form of a bi-static/multi-static radar system. The illuminators of opportunity are given priority to cover urban area, the received signal contains direct path signals, strong clutters, and target echoes. The experimental system is composed of a polarized antenna array, a receiver, an optical fiber board, and an upper computer. The radar system is shown in Fig. 18.

The antenna array is composed of three pairs of orthogonal polarization antennas. Each pair of polarized antenna requires two receiving channels. The polarization isolation reaches 20 dB between the frequency band 710 and 718 MHz, and the gain of each antenna is about 10 dB [28]. The receiver is composed of GPS receiving card, analog frontend, and digital acquisition. The optical fiber card converts electrical signals into optical signals and realizes high-speed data transmission.

Experimental result

AW-PSF is a signal fusion method based on adaptive weighting. After array calibration, interference suppression, and matched filtering, the data of H and V channels are adaptively weighted and fused, and the fused signal is detected with a constant false-alarm rate. The detection method is CA-CFAR, and the false-alarm rate is 10^{-6} . The detection target was a Boeing 737 plane which took off from the airport. The experimental scenario during airplane detection is shown in Fig. 19.

In Fig. 19, the green sector area represents the direction of polarized surveillance antenna beam. The blue sector area represents the direction of reference antenna beam. The yellow elliptical area represents plain. We use time domain and spatial domain interference suppression algorithms to suppress interference and clutter signals [11]. Then, we use different polarization signal fusion methods to fuse the target signal. We collected 112 frames of data. The data in one frame contain 40 timeslots, and the duration is 1 s. A timeslot contains 53 OFDM blocks. Each OFDM block contains a CP and a useful symbol portion. The useful symbol duration is 409.6 μ s. When the transmit mode of the opportunistic illumination source is V polarization, we compare the detection results after using single V or H polarization reception, using the P-NCI and AW-PSF as shown in Fig. 20.

It can be observed from the comparison results in Fig. 20 that the detection performance of the DPPR system is the best when

Table 5. Comparison of experimental results

Mode	Data length (frame)	Detection probability (%)	Performance improvement (%)
V	112	43.8	8.9(V) 15.2(H)
H		37.5	10.8(P-NCI)
P-NCI		41.9	
AW-PSF		52.7	

the AW-PSF is adopted. The results of specific experimental analysis are shown in Table 5.

In this experiment, the total length of data to be detected is 112 frames. When the AW-PSF method is adopted, the target can be detected in 59 frames of data, and the detection probability is 52.7%. The detection probability of AW-PSF is 8.9 and 15.2% higher than that of the single V polarization and H polarization modes, respectively, and 10.8% higher than that of the P-NCI method.

Conclusion

In this paper, we propose an adaptive weighting-based polarization signal fusion method. We compare the target detection performances of different polarization signal fusion methods. The proposed AW-PSF outperforms the single-polarization mode and the signal fusion P-NCI method.

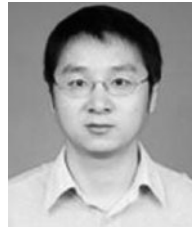
The RCS and PAR characteristic of target has also been studied in this paper. The RCS and PAR characteristic of Boeing 737 fluctuates dramatically. This means that not only the polarization filtering technology, but also the polarization fusion technology based on the polarization-scattering characteristics of the target can effectively improve the detection performance of DPPP systems.

Acknowledgement. The authors acknowledge Wuhan University for supporting the work of this paper. This study was supported by the National Nature Science Foundation of China (61967007 and 61963016), the Key Research and Development Program of Jiangxi Province (20202BBEL53014 and 20201BBF61012), the Natural Science Foundation of Jiangxi Province (20212BAB202005), the Research Project of National Defence Science and Technology Key Laboratory Foundation (6142113180101), and the Jiangxi Province Department of Education Science and Technology Research Key Project (GJJ200667, GJJ170360, and GJJ200667).

References

- Xie DQ, Yi JX, Shen J and Wan XR (2018) Experimental Research of Multi-FM Based Passive Radar. 2018 12th International Symposium on Antennas, Propagation and EM Theory (ISAPE), Hangzhou, China, 1–5.
- Schüpbach C, Paine S and O'Hagan D (2020) Efficient Direct Signal Cancellation for FM-based Passive Radar. 2020 IEEE Radar Conference (RadarConf20), Florence, Italy, 1–5.
- Plotka M, Malanowski M, Samczyński P, Kulpa K and Abratkiewicz K (2020) Passive Bistatic Radar Based on VHF DVB-T Signal. 2020 IEEE International Radar Conference (RADAR), Washington, DC, USA, 596–600.
- Vorobev E, Veremyev V and Tulenkov N (2019) Experimental DVB-T2 Passive Radar Signatures of Small UAVs. 2019 Signal Processing Symposium (SPSymposium), Krakow, Poland, 67–70.
- Kulpa K, Osiński B, Gromek D, Samczyński P, Malanowski M and Bączyk M (2019) Ground Clutter Stability Analyses in DAB based Passive Radar. 2019 Signal Processing Symposium (SPSymposium), Krakow, Poland, 146–149.
- Schüpbach C, Patry C, Maasdorp F, Böniger U and Wellig P (2017) Micro-UAV detection using DAB-based passive radar. 2017 IEEE Radar Conference (RadarConf), Seattle, WA, USA, 1037–1040.
- Yamada H and Ogawa T (2020) Human Location Estimation by Passive Radar Using WLAN Access Point. 2020 IEEE Asia-Pacific Microwave Conference (APMC), Hong Kong, 84–85.
- Rong J, Liu FF, Liu QH and Long T (2019) Coherent Integration Technique for Small Targets in Passive Radar Based on LTE Signals. 2019 IEEE International Conference on Signal, Information and Data Processing (ICSIDP), Chongqing, China, 1–5.
- Yi YC, Wan XR, Yi JX and Cao XM (2018) Polarization diversity technology research in passive radar based on subcarrier processing. *IEEE Sensors Journal* **19**, 1710–1719.
- Wan XR, Yi JX, Zhao ZX and Ke HY (2014) Experimental research for CMMB-based passive radar under a multipath environment. *IEEE Transactions on Aerospace and Electronic Systems* **50**, 70–85.
- Yi JX, Wan XR, Li DS and Leung H (2018) Robust clutter rejection in passive radar via generalized subband cancellation. *IEEE Transactions on Aerospace and Electronic Systems* **54**, 1931–1946.
- Filippini F and Colone F (2017) A practical approach to polarimetric adaptive target detection in passive radar, International Conference on Radar Systems (Radar 2017), Belfast, 1–6.
- Colone F and Lombardo P (2016) Non-coherent adaptive detection in passive radar exploiting polarimetric and frequency diversity. *IET Radar, Sonar & Navigation* **10**, 15–23.
- You J, Wan XR, Fu Y and Fang G (2015) Experimental study of polarisation technique on multi-FM-based passive radar. *IET Radar, Sonar & Navigation* **9**, 763–771.
- Filippini F and Colone F (2020) Polarimetric passive radar: a practical approach to parametric adaptive detection. *IEEE Transactions on Aerospace and Electronic Systems* **56**, 4930–4946.
- Filippini F and Colone F (2019) Polarimetric Detection Scheme for Passive Radar based on a 2D Auto-Regressive Disturbance Model, 2019 International Radar Conference (RADAR), Toulon, France, 1–6.
- Conti M, Moscardini C and Capria A (2016) Dual-polarization DVB-T Passive Radar: Experimental Results, IEEE Radar Conference, Philadelphia, PA, USA.
- Zeng YH, Ai XF, Wang LD, Wang XY and Zheng GY (2016) Experimental research of dual-polarization passive radar based on DTTB signal. *Journal of Computer and Communications* **4**, 101–107.
- Filippini F, Colone F, Cristallini D and Bournaka G (2017) Preliminary experimental results of polarimetric detection schemes for DVB-T based passive radar, 2017 IEEE Radar Conference (RadarConf), Seattle, WA, USA, pp. 383–388.
- Wojaczek P, Cristallini D, Schell J, O'Hagan D and Summers A (2020) Polarimetric Antenna Diversity for Improved Reference Signal Estimation for Airborne Passive Radar, 2020 IEEE Radar Conference (RadarConf20), Florence, Italy, 1–6.
- Yi YC, Wan XR, Yi JX and Cao XM (2018) Polarisation experimental research of passive radar based on digital television signal. *IET Electronics Letters* **54**, 385–387.
- Ai XF, Zeng YH, Gao L, Wang XY and Wang LD (2016) Research on full-polarization bistatic scattering characteristics of aircraft. *Journal of Radars* **5**, 639–646.
- Ren B, Shi LF and Wang GY (2016) Statistical properties of the polarisation ratio for dual-polarisation radar operating at simultaneous reception mode. *IET Radar, Sonar & Navigation* **10**, 870–876.
- Nagy LL and Mich W (1977) Polarized radar system for providing target identification and discrimination. US Patent 4035797/1977.
- Bongioanni C, Colone F, Martelli T, Angeli RD and Lombardo P (2010) Exploiting Polarimetric Diversity to Mitigate the Effect of Interferences in FM-based Passive Radar, IEEE International Radar Symposium, Vilnius, Lithuania.
- Bongioanni C, Colone F and Lombardo P (2008) Performance Analysis of a Multi-frequency FM based Passive Bistatic Radar, IEEE Radar Conference, Rome, Italy.

27. **Griffiths HD and Baker CJ** (2005) Passive coherent location radar systems. Part 1: performance prediction. *IEEE Proceedings-Radar, Sonar and Navigation* **152**, 153–159.
28. **Cao XM, Gong ZP, Yi YC and Wang BJ** (2016) Design of a Dual-Polarized Yagi-Uda Antenna for the Passive Radar, IEEE 11th International Symposium on Antennas, Propagation and EM Theory, Guilin, China.



Lu Zhu was born in Jiangxi, China, in 1976. He received his Ph.D. degree from the Huazhong University of Science and Technology. He is now a professor and Master supervisor at the School of Information Engineering, East China Jiaotong University. In recent years, he has hosted and participated in more than 10 national research projects.



Yucheng Yi was born in Hunan, China, in 1985. He received his Ph.D. degree from the School of Electronic Information, Wuhan University. He is now a lecturer at the School of Information Engineering, East China Jiaotong University. His main research interests include radar signal processing and polarization array signal processing.



Xiaomao Cao was born in Hunan, China, in 1991. He is currently working toward his Ph.D. degree at the School of Electronic Information, Wuhan University. His main research interests include radar signal processing, antenna design, and array calibration.